



### **Science Arts & Métiers (SAM)**

is an open access repository that collects the work of Arts et Métiers Institute of Technology researchers and makes it freely available over the web where possible.

This is an author-deposited version published in: <https://sam.ensam.eu>  
Handle ID: <http://hdl.handle.net/10985/24987>

#### **To cite this version :**

Sara ZANCHI, Sébastien ROLAND, Lena LE GOFF, Damien THUAU, Pierre MARGERIT, Marc RÉBILLAT, Ilias ILIOPOULOS, Sylvie TENCÉ-GIRAULT - Smart actuators based on electroactive fluorinated polymers: relationship between molecular organization and electroactive response - In: SMART2023 (10th Eccomas Thematic Conference on Smart Structures and Materials, 2023-07-03-05 Greece), Grèce, 2023-07-03 - SMART 2023 (10th Eccomas thematic conference on Smart Structures and Materials) - 2023

Any correspondence concerning this service should be sent to the repository

Administrator : [scienceouverte@ensam.eu](mailto:scienceouverte@ensam.eu)



# SMART ACTUATORS BASED ON ELECTROACTIVE FLUORINATED POLYMERS: RELATIONSHIP BETWEEN MOLECULAR ORGANIZATION AND ELECTROACTIVE RESPONSE

S. ZANCHI,<sup>1</sup> S. ROLAND,<sup>1\*</sup> L. LE GOFF,<sup>1</sup> D. THUAU,<sup>3</sup> P. MARGERIT,<sup>1</sup>  
M. REBILLAT,<sup>1</sup> I. ILIOPOULOS,<sup>1</sup> S. TENCÉ-GIRAULT<sup>1,2</sup>

<sup>1</sup> Laboratoire PIMM, Arts et Métiers Institute of Technology, CNRS, Cnam, HESAM Université,  
151 bd de l'Hôpital, 75013 Paris, France

<sup>2</sup> Arkema, CERDATO, Route du Rilsan, 27470 Serquigny, France

<sup>3</sup> Laboratoire IMS, Université de Bordeaux, CNRS Bordeaux INP/ENSCBP,  
351 Cours de la Libération, 33400 Talence, France

[\\*sebastien.roland@ensam.eu](mailto:*sebastien.roland@ensam.eu)

## Abstract.

Electroactive polymers (EAP) show a change of properties (size, shape, temperature...) when an electric field is applied. Poly(vinylidene fluoride-*ter*-trifluoroethylene-*ter*-chlorotrifluoroethylene) P(VDF-*ter*-TrFE-*ter*-CTFE) terpolymers have been extensively studied since the 2000s and they found various applications in organic printed and flexible electronics, such as smart actuators. They exhibit different electroactive properties depending on the CTFE content. For %CTFE = 0, copolymers are ferroelectric and piezoelectric at room temperature (RT), while terpolymers are relaxor-ferroelectric and electrostrictive at RT for %CTFE > 6%. On the top of the processing conditions, the chemical composition (%CTFE) have a strong impact on the crystalline structure and morphology, and consequently on the electroactive properties. Unimorph actuators with two different chemical compositions were studied by in-situ Wide Angles X-Ray Scattering (WAXS) and by measuring their macroscopic deformation under an increasing electric field (up to 110 V/μm). These techniques were used to extract their electromechanical coefficients ( $d_{31}$  and  $Q_{31}$ ) at the macroscopic scale and to relate the crystalline scale to the macroscopic properties. By comparing the evolution of the crystalline unit cell dimensions and of the macroscopic strain of the actuator under an electric field, interesting information on the mechanisms involved were deduced and will be discussed.

**Key words:** VDF-based polymers, smart actuator, electroactive

## 1 INTRODUCTION

In the last decades, printed organic electronics have attracted increasing interest for various applications, such as actuators. The use of electroactive polymers (EAPs) in these devices provides numerous benefits such as flexibility, light weight, low cost, and ease of miniaturization. Fluorinated electroactive polymers have been extensively studied for application in the field of organic electronics, due to their unique electroactive properties [1,2]. While P(VDF-*co*-TrFE) copolymers exhibit piezoelectric behavior under an electric field,

P(VDF-*ter*-TrFE-*ter*-CTFE) terpolymers show electrostrictive behavior. In the former, the induced strain is proportional to the electric field, while in the latter, it is quadratic to the electric field. One of the simplest actuator geometries is the unimorph, where both electrodes and the active layer are printed on the same side of a passive structural substrate. Processing conditions and the chemical composition of the electroactive layer strongly impact the crystalline structure and morphology, and therefore, the macroscopic properties of the device [3,4]. Thus, it is crucial to understand the in-situ behavior of these actuators under an electric field at a multi-scale level. Few studies that combine microscopic and macroscopic scales exist in the literature. Several recent studies have focused on measuring crystal lattice deformation to explain piezoelectric or electrostrictive movements in various types of PVDF-based polymers, including biaxially stretched PVDF, P(VDF-*co*-TrFE) copolymers, and P(VDF-*ter*-TrFE-*ter*-CTFE) terpolymers [5–7]. However, each study has its own limitations. Lheritier et al. compared in-situ WAXS analyses with macroscopic displacement and strain measurements, but the use of different substrates for the two analyses made the comparison less ideal.[5] Katsouras et al. measured crystal lattice deformation in P(VDF-*co*-TrFE) copolymers that were spin-coated on quartz substrates, while Tashiro et al. measured deformation in biaxially stretched PVDF homopolymers [6,7]. These studies primarily focused on crystal lattice deformations measured using X-ray analyses, without comparing them with macroscopic strains, except for those extracted from the literature.

In contrast, the current study aims to measure both electromechanical deformation at the crystalline scale and macroscopic scale on the same object, which happens to be an actuator.

## 2 EXPERIMENTAL SECTION

### 2.1. Manufacturing of the actuator

For this study, two polymer powders (provided by Arkema-Piezotech) were selected with a similar VDF/TrFE ratio ( $\sim 65/35$ ) and containing 0 mol % and 8.3 % mol of CTFE monomer, respectively. To obtain homogeneous inks, the polymer powders were dissolved in triethylphosphate at 18 wt % using a reflux setup at 80 °C for 3 h and filtered with a 1  $\mu\text{m}$  mesh. Poly(3,4-ethylenedioxythiophene) polystyrene sulfonate (PEDOT:PSS) (Clevios PH1000) purchased from Heraeus was used to create the top and bottom electrodes. A 25  $\mu\text{m}$  thick film of amorphous poly(ether ketone ketone) (PEKK) was chosen as a substrate (provided by Arkema), and all the layers of the device were screen-printed on the same side of the substrate as shown in Figure 1a. After each layer was printed, an annealing of 15 minutes at 100-110 °C was performed to allow the solvent to evaporate. The two actuators underwent an overall one-hour annealing at  $T_m - 15$  °C. The final devices are unimorph actuators with an active area of 4 mm x 10 mm. The two actuators were named TerpoX-Y, where X refers to the VDF/(TrFE + VDF) ratio and Y to the amount of CTFE (mol %), so Terpo65-0 and Terpo67-8.3.

### 2.2. Electric displacement-Electric field loops

*D-E* loops were recorded with a TF Analyzer 2000 (aixACCT System). *D-E* loops of thin films ( $\sim 4$   $\mu\text{m}$ ) of diverse compositions were measured directly onto the actuators as integrated current versus electric field, which was swept as a sinusoidal voltage waveform up to about 110 V/ $\mu\text{m}$  at a frequency of 1 Hz between both bottom and top electrodes.

### 2.3. Macroscopic deformation of the actuator

The experimental setup used for this study is illustrated in Figure 1b. An electric system, including a voltage source, a voltage amplifier, and an oscilloscope was used to apply a sinusoidal electric signal to the actuator, which was clamped on the side of electric connections and free on the other end. A camera was positioned above the actuator to capture its bending motion under the electric field. Subsequently, the videos of the actuators were processed using a Matlab code, which detected the lateral section of the actuator as a line and tracked the vertical displacement of the actuator tip under the external electric field.

From a mechanical perspective, the unimorph actuator consists in a cantilever with a uniformly distributed load, i.e. the electric field. A scheme of its bending under electric field is presented in Figure 1c. The deflection  $\eta$  at the cantilever tip can be expressed as follows:

$$\eta = \frac{1}{2} \alpha L^2 \quad (1)$$

where  $\alpha$  is the curvature of the unimorph and  $L$  its length. Under this assumption, the Abe model for the displacement control of an electrostrictive unimorph actuator can be applied to calculate the cross deformation ( $S_{31}$ ) of the EAP layer under the external electric field, according to the following formula [8]:

$$\alpha = \frac{2Y_{EAP}t_{EAP}S_{31}}{Y_{PEKK}[t_0^2 - (t_0 - t_{PEKK})^2] + Y_{EAP}[(t_0 + t_{EAP})^2 - t_0^2]} \quad (2)$$

where  $Y_{EAP}$ ,  $Y_{PEKK}$  are the Young's moduli of the EAP layer and the (PEKK) substrate, respectively;  $t_{EAP}$  and  $t_{PEKK}$  are the thicknesses of the EAP layer and the substrate, respectively;  $t_0$  is the thickness of the neutral layer where the strain is null, and is defined as follows:

$$t_0 = \frac{t_p t_s^2 (3t_p + 4t_s) Y_s + t_p^4 Y_p}{6t_s t_p (t_p + t_s) Y_s} \quad (3)$$

Thanks to these formulae,  $d_{31}$  and  $Q_{31}$  coefficients can be calculated for piezoelectric and electrostrictive behaviors, respectively, using the following equations:

$$S_{31} = d_{31} E \quad (4)$$

$$S_{31} = Q_{31} D^2 \quad (5)$$

$d_{31}$  and  $Q_{31}$  coefficients are determined at low  $E$  and over the whole  $D^2$  range, respectively.

### 2.4. Microscopic deformation of the actuator

In-situ WAXS analyses were performed on the SWING beamline at Soleil Synchrotron to measure the evolutions of the crystalline lattice under an electric field (project n°: 20210035). The beam energy was set at 10 keV, resulting in a wavelength of 1.24 Å. The experimental setup is shown in Figure 1d. WAXS patterns were recorded using a Merlin detector (Quantum Detectors) positioned at 0.092 m from the sample in air, covering a  $q$  range between 0.9 Å<sup>-1</sup> and 3.6 Å<sup>-1</sup>. WAXS acquisitions were performed during increasing and decreasing ramps of the electric field, with a step of 11 V/μm and an acquisition plateau of 100 ms. Simultaneously, the sample was mapped to prevent dielectric breakdowns [7]. The reduction of 2D pattern from

the Merlin detector to 1D was achieved by radially averaging the 2D images using Foxtrot software. The WAXS spectra were then normalized by the acquisition time and by the number of transmitted photons. The normalized WAXS spectrum acquired on the PEKK substrate with PEDOT:PSS electrodes was subtracted.

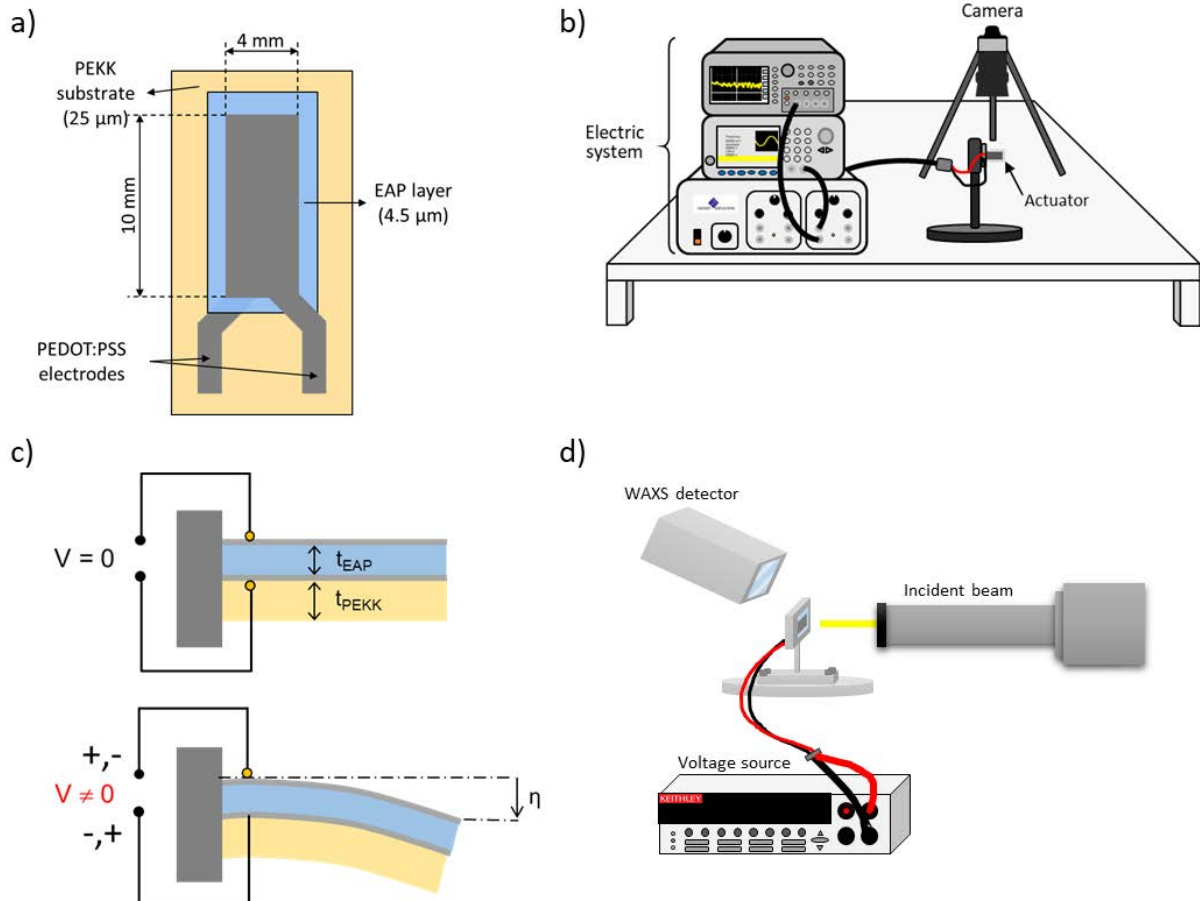


**Figure 1:** a) Scheme of the actuator with its layers (top view), b) experimental setup for the measurement of the macroscopic deflection of the actuator, c) scheme of the cross-section of the actuator before and during the application of an external electric field, and d) experimental setup for the in-situ WAXS analyses at Soleil synchrotron.

### 3 RESULTS AND DISCUSSION

#### 3.1. Macroscopic deformation under electric field

The electric displacement-electric field (D-E) loops of the two actuators are depicted in Figure 2a. Terpo65-0 (black curve) has a coercive field,  $E_c$ , of 53 V/μm and a remnant polarization,  $P_r$ , of 61 mC/m<sup>2</sup>. Terpo67-8.3 (green curve) exhibits  $E_c$  and  $P_r$  values of 13 V/μm and 9 mC/m<sup>2</sup>, respectively. These values illustrate the distinct responses of the two actuators to an external electric field, as their active layers contain varying amounts of CTFE: Terpo65-0 is ferroelectric (FE), while Terpo67-8.3 is relaxor ferroelectric (RFE). Since the FE behavior is associated with piezoelectric deformation and the RFE behavior is coupled with electrostrictive deformation, the two unimorph actuators exhibit different bending behaviors under an electric

field. Figure 2b displays the deflection of the tip ( $\eta$ ) relative to the applied electric field is shown in. The  $\eta$  values for Terpo65-0 (black curve) can be positive or negative, as the deflection occurs in both directions (piezoelectricity), resulting in a butterfly loop. The  $\eta$ -E loop for Terpo67-8.3 (green curve) only shows positive deflection values since the active layer of this actuator has an electrostrictive behavior. The maximum deflection value is approximately 3 mm for both actuators.

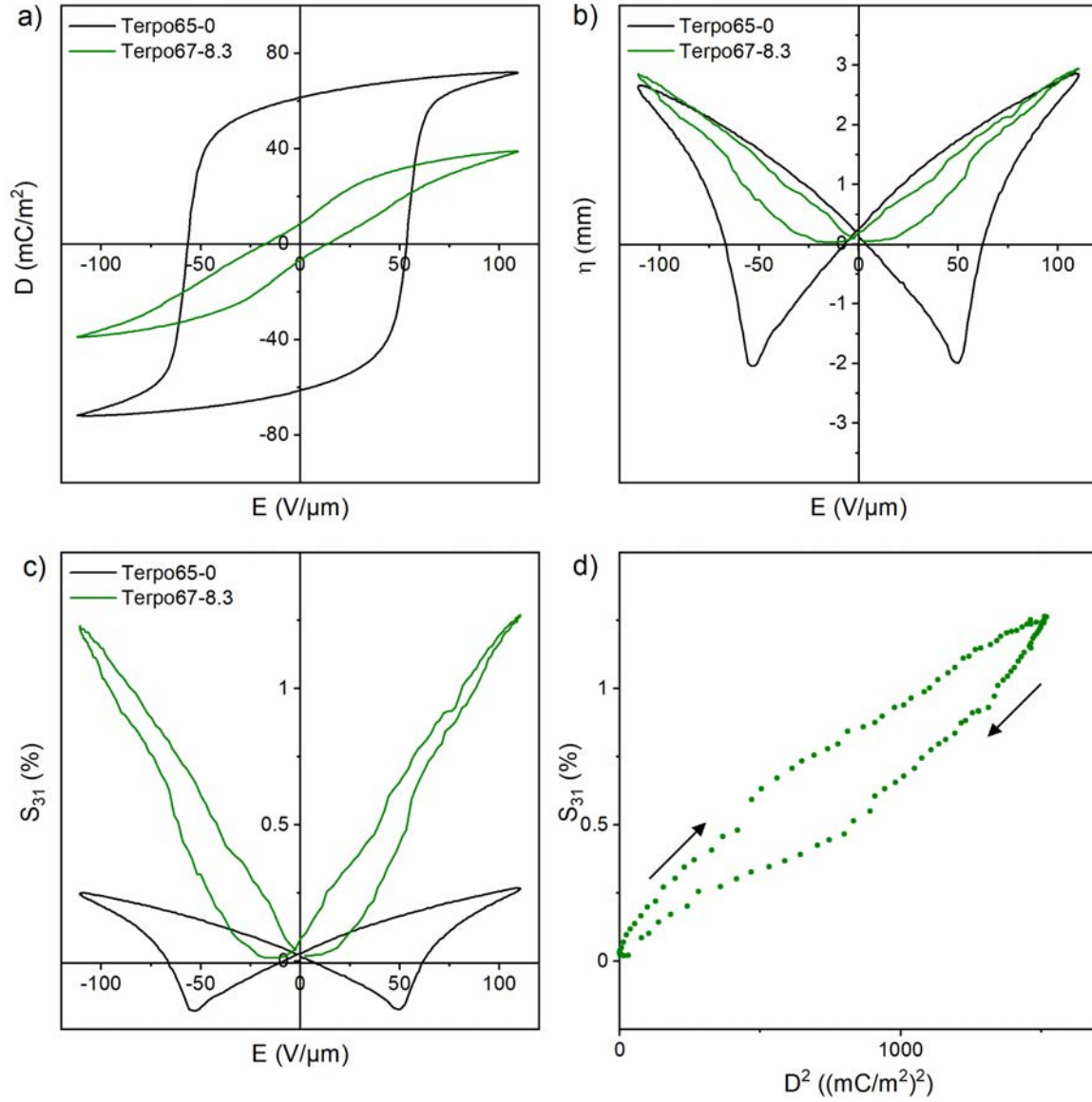


**Figure 2:** a) Electric displacement-electric field ( $D$ - $E$ ) loops, b) deflection-electric field ( $\eta$ - $E$ ) loops, and c) cross deformation-electric field ( $S_{31}$ - $E$ ) loops for Terpo65-0 and Terpo67-8.3 actuators. d) Evolution of  $S_{31}$  with respect to  $D^2$  for Terpo67-8.3.

Using the Abe model for unimorph actuators, the cross deformation ( $S_{31}$ ) of the active layer under an electric field was obtained. The results are shown in Figure 2c: Terpo67-8.3 exhibits

the highest  $S_{31}$  value, reaching ca. 1.25% at an electric field of 110 V/ $\mu\text{m}$ , while the deformation of the Terpo65-0 actuator remains below 0.3%. Since  $S_{31}$  is directly proportional to the electric field, the piezoelectric coefficient  $d_{31}$  can be calculated as the slope of the  $S_{31}$ -E plot, which was found to be 33 pm/V. To determine the electrostrictive coefficient  $Q_{31}$  for Terpo67-8.3, another step is needed since  $S_{31}$  is proportional to the squared electric displacement. Figure 2d shows the evolution of the cross deformation of the active layer with respect to  $D^2$ . The data points were collected while increasing the electric field from 0 V/ $\mu\text{m}$  up to  $E_{\text{max}}$  and then decreasing it from  $E_{\text{max}}$  back to 0 V/ $\mu\text{m}$ . The slope of the first series of points yields an electrostrictive coefficient of ca.  $7 \text{ m}^4 \text{ C}^{-2}$ .

### 3.2. In-situ WAXS experiments

#### *P(VDF-co-TrFE) actuator*

In Figure 3, the in-situ WAXS data is plotted as a function of the electric field in a 3D graph. First, an increase in the field up to  $E_{\text{max}}$  ( $\sim 110 \text{ V}/\mu\text{m}$ ), followed by a decrease to 0 V/ $\mu\text{m}$ , was applied to the actuator. After normalization and subtraction of the substrate and electrode contributions, the WAXS data are plotted for a restrained wave vector domain between  $1.1 \text{ \AA}^{-1}$  and  $1.6 \text{ \AA}^{-1}$ . In Figure 3, an increase in the intensity of the Bragg peak located around  $1.4 \text{ \AA}^{-1}$  is observed and this increase is non-reversible when the electric field decreases to 0 V/ $\mu\text{m}$ . A decomposition of the WAXS spectrum was performed using Fityk [9] in order to extract the intensities and positions of the main Bragg peaks. In Figure 4b-c, the relative intensities  $I_{\text{FE}}/(I_{\text{FE}}+I_{\text{DFE}})$  and  $I_{\text{DFE}}/(I_{\text{FE}}+I_{\text{DFE}})$  of the FE et DFE phases, as well as the interplanar distances  $d_{\text{FE}}$  et  $d_{\text{DFE}}$  ( $d = 2\pi/q_{\text{max}}$ ) of these phases, are plotted as a function of the electric field (E). These different evolutions are compared to the evolution of the polarization (P) during a similar electric field ramp in Figure 4.

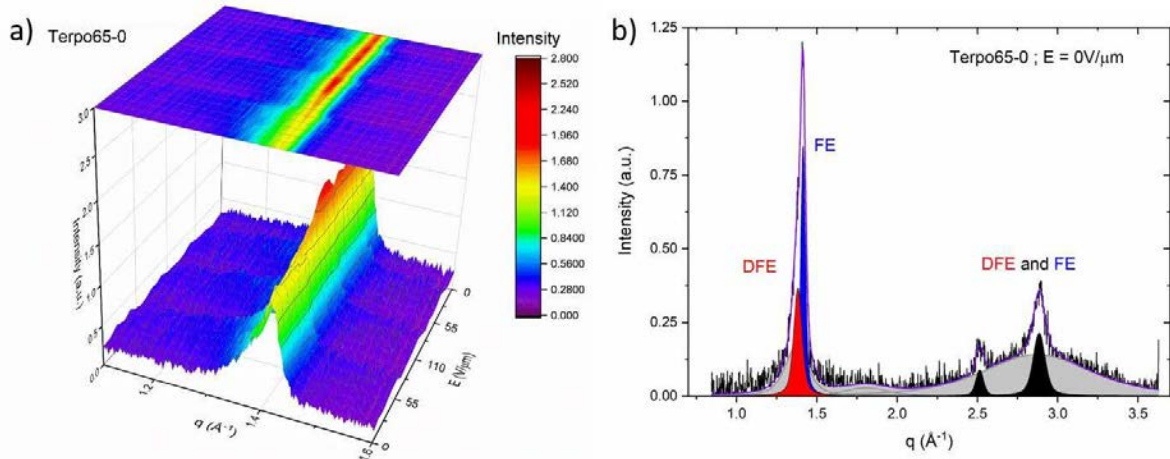


**Figure 3:** In-situ WAXS diffraction experiment under an electric field. a) 3D representation, showing a zoom of the WAXS spectra in the  $q$  range between  $1.1$  and  $1.6 \text{ \AA}^{-1}$ ; b) WAXS spectra of Terpo65-0 for  $E = 0 \text{ V}/\mu\text{m}$ , with the decomposition in amorphous (gray) and crystalline peaks. The red and blue peaks are the main inter-chain diffraction peaks of the DFE and FE phases respectively. The small black peaks are associated with the intra- and inter-chain distances mostly of the FE phase.



A progressive decrease in the intensity of the DFE Bragg peak is observed, associated with an increase in the intensity of the FE peak, as the electric field is increased. No evolution is observed during the decrease of the electric field. This non-reversibility of the intensity evolution reflects the evolution observed in Figure 3a. Simultaneously, the interplanar distance,  $d_{FE}$  increased from 4.44 Å to 4.46 Å and this increase is non-reversible upon decreasing the electric field. These observations indicate that a significant fraction of the DFE phase is polarized into the FE phase under an electric field. The experimental results presented here allow for the *in-situ* visualization of the evolution of the WAXS spectra, from a non-polarized to a polarized state [10].

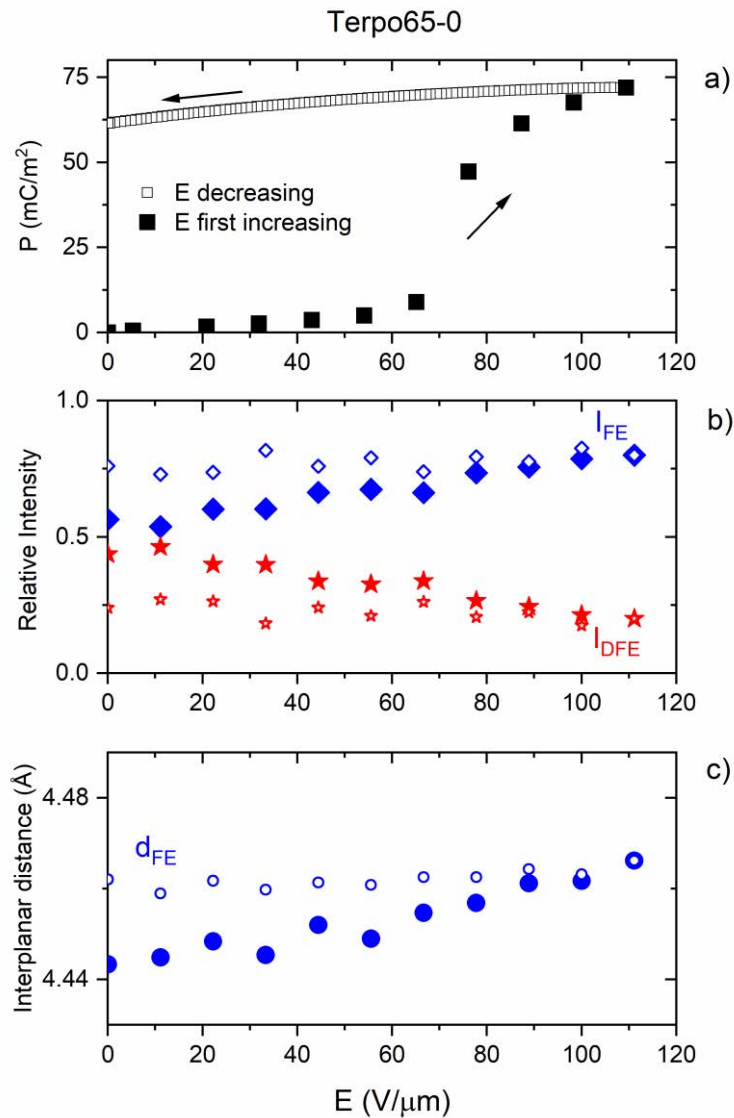


**Figure 4:** Structural evolution of the Terpo65-0 actuators under an electric field (E): first, E was gradually increased up to 110 V/μm, followed by a decrease back to 0 V/μm. a) Polarization, b) relative intensity of the DFE and FE Bragg peaks, and c) interplanar distance  $d_{FE} = d_{200}/d_{110}$  of the FE phase.



### *P(VDF-ter-TrFE-ter-CTFE)* actuator

The same experimental protocol was implemented for the Terpo67-8.3 actuator, and the results are shown in Figure 5 and 6. In Figure 5a, the 3D representation of the WAXS spectra as a function of the electric field clearly shows a reversible evolution, with a distinct WAXS spectrum at high electric field. This reversible behavior is consistent with the relaxor-ferroelectric properties of a terpolymer containing 8.3 mol% CTFE [3].

The WAXS spectrum of the Terpo67-8.3 actuator (Figure 5b) is different from that of the Terpo65-0. Specifically, the Bragg peaks between 2.5 et 3  $\text{\AA}^{-1}$ , which primarily originate from the intra-chain order, are absent for the terpolymer. Additionally, around 1.4  $\text{\AA}^{-1}$ , the two contributions of the orthorhombic RFE phase, the (200) line and the (110) line, are now separated. We monitored the evolution of their relative intensities,  $I_{200}$  and  $I_{110}$ , and interplanar distances,  $d_{200}$  and  $d_{110}$ , with the electric field (Figure 6).

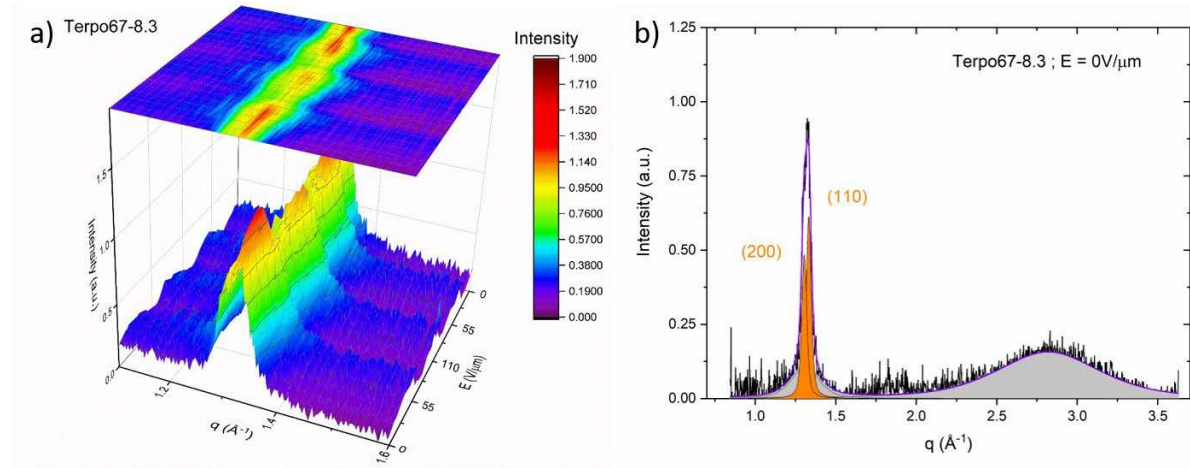


**Figure 5:** In-situ WAXS diffraction experiment under an electric field. a) 3D representation, showing a zoom of the WAXS spectra in the  $q$  range between 1.1 and 1.6  $\text{\AA}^{-1}$ ; b) WAXS spectra of Terpo67-8.3 for  $E = 0 \text{ V}/\mu\text{m}$ , with the decomposition in amorphous (gray) and crystalline peaks. The two orange peaks are associated with the inter-chain distances (200) and (110) of the RFE phase.

Figure 6 shows the roughly reversible evolutions with respect to the electric field ( $E$ ), for the polarization ( $P$ ), the relative intensities ( $I_{200}$ ,  $I_{110}$ ) and the interplanar distances ( $d_{200}$ ,  $d_{110}$ ). The evolution of the relative intensities reflects, among other things, an orientation of the dipoles and thus of the crystalline planes under the application of the electric field, while the evolution of the interplanar distances represents a continuous and reversible decrease of the  $b$  cell parameter and a simultaneous increase of the  $a$  cell parameter. These evolutions are in full agreement with a progressive orientation of the dipoles in the direction of the electric field.

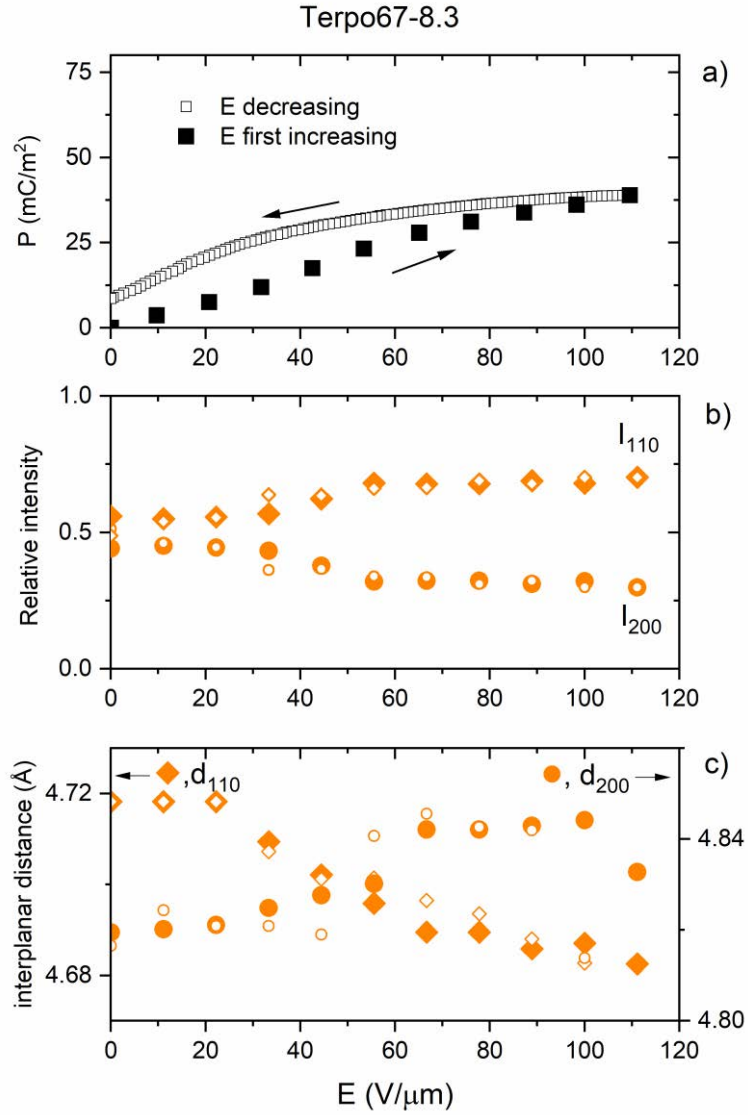


**Figure 6:** Structural evolution of the Terpo67-8.3 actuators under electric field (E): first, E was gradually increased up to 110 V/μm, followed by a decrease back to 0 V/μm. a) Polarization b) relative intensity of the (200) and (110) Bragg peaks of the RFE phase c) inter planar distances  $d_{110}$  and  $d_{200}$  of the RFE phase.

#### 4 CONCLUSIONS

This study focuses in the correlation of macroscopic phenomena, such as deformations and measurements of  $d_{31}$  and  $Q_{31}$  coefficients, with the polarization and evolution of interplanar distances in DFE, FE, and RFE crystalline phases, all measured on the same object: a unimorph actuator designed and built for these specific experiments.

The irreversibility of the polarization of the copolymer under an electric field of 110 V/μm is associated with the irreversible transition under electric field from the DFE phase to the FE phase. The measured deformation of the interplanar distance  $d_{FE}$  is very low, consistent with the macroscopic variation of less than 0.3% (Figure 2c), which leads to the coefficient

$d_{31} \sim 33 \cdot 10^{-12}$  C/N. On the other hand, the reversible evolution of the terpolymer Terpo67-8.3 under an electric field leads to larger macroscopic and interplanar deformations, around 1% (Figure 2d), resulting in a  $Q_{31} \sim 7$  m<sup>4</sup>/C<sup>2</sup>.

It is not intuitive to understand how this 1% deformation of the interplanar distances within the crystalline lamellae leads to a macroscopic deformation of the same order of magnitude (1%). In particular, one may wonder how the amorphous phase, which represents about 80% of the volume of the sample, evolves.

## 5 ACKNOWLEDGMENTS

This research was carried out within the framework of the Industrial Chair Arkema (Arkema/CNRS-ENSAM-Cnam, Arkema N° AC-2018-413, CNRS N° 183697). This work was partially funded by the French National Research Agency (ANR FETA project, ANR-18-CE06-0024). We are grateful to the SOLEIL synchrotron facility and the SWING beamline for access to their instrumentation (project n° 20210035). We extend our warmest thanks to beamline manager, Javier Perez, for his advice before and assistance during the in-situ experiments.

## REFERENCES

- [1] S. G. Lu, X. Chen, T. Levard, P. J. Diglio, L. J. Gorny, C. D. Rahn, and Q. M. Zhang, “Large Displacement in Relaxor Ferroelectric Terpolymer Blend Derived Actuators Using Al Electrode for Braille Displays,” *Sci. Rep.*, vol. 5, no. 1, p. 11361, Jun. 2015, doi: 10.1038/srep11361.
- [2] S. T. Choi, J. Y. Lee, J. O. Kwon, S. Lee, and W. Kim, “Varifocal liquid-filled microlens operated by an electroactive polymer actuator,” *Opt. Lett.*, vol. 36, no. 10, p. 1920, May 2011, doi: 10.1364/OL.36.001920.
- [3] F. Bargain, D. Thuau, G. Hadziioannou, F. Domingues Dos Santos, and S. Tencé-Girault, “Phase diagram of poly(VDF-ter-TrFE-ter-CTFE) copolymers: Relationship between crystalline structure and material properties,” *Polymer*, vol. 213, p. 123203, Jan. 2021, doi: 10.1016/j.polymer.2020.123203.
- [4] S. Zanchi, M. Engel, A. Pascaud, F. Bargain, S. Lebreton, F. Domingues dos Santos, S. Roland, and S. Tencé-Girault, “Unraveling the morphological diversity of P(VDF-ter-TrFE-ter-CTFE) semi-crystalline terpolymers via combined AFM and SAXS experiments,” *Polym. Test.*, vol. 120, p. 107973, Mar. 2023, doi: 10.1016/j.polymertesting.2023.107973.
- [5] P. Lheritier, N. Vaxelaire, S. Tencé-Girault, F. Domingues Dos Santos, and E. Defay, “Influence of Field-Induced Phase Transition on Poly(Vinylidene Fluoride-Trifluoroethylene-Chlorotrifluoroethylene) Strain,” *Phys. Rev. Appl.*, vol. 14, no. 4, p. 044061, Oct. 2020, doi: 10.1103/PhysRevApplied.14.044061.
- [6] I. Katsouras, K. Asadi, M. Li, T. B. van Driel, K. S. Kjær, D. Zhao, T. Lenz, Y. Gu, P. W. M. Blom, D. Damjanovic, M. M. Nielsen, and D. M. de Leeuw, “The negative piezoelectric effect of the ferroelectric polymer poly(vinylidene fluoride),” *Nat. Mater.*, vol. 15, no. 1, Art. no. 1, Jan. 2016, doi: 10.1038/nmat4423.
- [7] K. Tashiro, H. Yamamoto, S. Kummara, D. Tahara, K. Aoyama, and H. Sekiguchi, “Electric-Field-Induced Phase Transition and Crystal Structural Change of the Oriented Poly(vinylidene Fluoride)  $\beta$  Form as Clarified by the In Situ Synchrotron Wide-Angle X-

- ray Diffraction Measurement,” *Macromolecules*, vol. 55, no. 15, pp. 6644–6660, Aug. 2022, doi: 10.1021/acs.macromol.2c01015.
- [8] Abe et al., “The Electrostrictive Unimorph for Displacement Control,” *Jpn. J. Appl. Phys.*, vol. 21, no. 7, pp. L408–L410, 1982.
- [9] M. Wojdyr, “Fityk: a general-purpose peak fitting program,” *J. Appl. Crystallogr.*, vol. 43, no. 5–1, pp. 1126–1128, 2010, doi: 10.1107/S0021889810030499.
- [10] F. Bargain, P. Panine, F. Domingues Dos Santos, and S. Tencé-Girault, “From solvent-cast to annealed and poled poly(VDF-co-TrFE) films: New insights on the defective ferroelectric phase,” *Polymer*, vol. 105, pp. 144–156, Nov. 2016, doi: 10.1016/j.polymer.2016.10.010.